Aggregate breakdown dynamics under rainfall compared with aggregate stability measurements

Cédric Legout, Sophie Leguédois, Yves Le Bissonnais

▶ **To cite this version:**

Cédric Legout, Sophie Leguédois, Yves Le Bissonnais. Aggregate breakdown dynamics under rainfall compared with aggregate stability measurements. European Journal of Soil Science, 2005, 56 (2), pp.225 à 238. 10.1111/j.1365-2389.2004.00663.x . insu-00383192

HAL Id: insu-00383192

https://insu.hal.science/insu-00383192

Submitted on 31 May 2020

HAL is a multi-disciplinary open access archive for the deposit and dissemination of scientific research documents, whether they are published or not. The documents may come from teaching and research institutions in France or abroad, or from public or private research centers.

L'archive ouverte pluridisciplinaire **HAL**, est destinée au dépôt et à la diffusion de documents scientifiques de niveau recherche, publiés ou non, émanant des établissements d'enseignement et de recherche français ou étrangers, des laboratoires publics ou privés.

Aggregate breakdown dynamics under rainfall compared to aggregate stability measurements

C. Legout[a,b], S. Leguédois[b] & Y. Le Bissonnais[b]

[a] *INRA, UMR Sol, Agronomie, Spatialisation, 65, rue de St Brieuc, 35042 Rennes Cedex & [b] INRA, Unité de Science du Sol, BP 20619 Ardon, 45166 Olivet CEDEX, France*

Correspondence: Cédric Legout. E-mail: cedric.legout@roazhon.inra.fr

Short running title: *Aggregate breakdown: temporal dynamics and stability*

Received 12 September 2003; revised version accepted 22 March 2004

Summary

Aggregate breakdown due to rainfall action causes crusting and interrill erosion. Erodibility is, seemingly, determined by the capacity of surface aggregates to resist the effects of rainfall. In this paper, we evaluated the relevance of an aggregate stability measurement, which comprises three treatments, in order to characterize aggregate breakdown dynamics. Two cultivated soils were studied: a clay loam slightly sensitive to erosion and a more susceptible silt loam. We compare the size distributions of micro-aggregates produced by the three aggregate stability treatments to the results from a rainfall simulation. The behaviour of four initial aggregate size classes (< 3 mm, 3-5 mm, 5–10 mm, and 10–20 mm) was also compared to study the influence of the initial aggregate size on the nature of resulting aggregates. The Mean Weight Diameter was from 200 to 1400 μm for the silt loam, and from 600 to 7000 μm for the clay loam. The two experiments, aggregate stability measurements and aggregate breakdown dynamics under rainfall, yielded similar results. Qualitative analysis showed that for both soils, the sizes of fragments produced by breakdown with the aggregate stability tests and under rainfall were similar and seemed to be qualitatively independent of the size of initial aggregates. We first schematized the structural organization of aggregates in cultivated horizons with a simple hierarchical model at two levels: (i) < 250 μm micro-aggregates, (ii) > 250 μm macro-aggregates made by the binding together of micro-aggregates. We then developed a model of aggregate breakdown dynamics under rainfall which gives, for various rainfall durations, the size distributions of resulting fragments on the basis of aggregate stability measurements. We obtained a correlation coefficient of 0.87 for the silt loam and of 0.91 for the clay loam, showing that the experimental and predicted mass percentages were linearly related for each size fraction.

Introduction

Crusting and interrill erosion on cultivated soils result from aggregate breakdown and transfer of soil fragments by rain and runoff. Aggregate stability influences several aspects of a soil's physical behaviour, in particular water infiltration and soil erosion. Sealing results in decreased infiltration and increased overland flow and erosion. The relationship between crusting and erosion was investigated by Hairsine & Hook (1994), who concluded that there was much in common between both processes, and that erosion rates were controlled in great part by aggregate breakdown processes. Soil erodibility can be estimated from some measured soil properties that are often correlated with erosion (Amézketa et al., 1996) such as texture (Bradford *et al.*, 1987), the percentage of Fe and Al (Le Bissonnais & Singer, 1993), exchangeable Ca or sum of exchangeable bases (Meyer & Harmon, 1984), exchangeable sodium (Emerson, 1967), and organic matter (Tisdall & Oades, 1982; Haynes, 1993). All these parameters have sometimes statistically significant relationships with soil erosion. In addition, statistical modelling is very difficult because of the large number of parameters and the complexity of their interactions.

An aggregate stability measurement combines and integrates the effect of all these textural and chemical parameters with their interactions in a single value. Various aggregate stability measurements have been proposed in order to predict soil surface behaviour and erosion (Le Bissonnais, 1996; Amézketa et al., 1996). The relationship between aggregate stability and erosion has generally been dealt with at an empirical level without considering the different aggregate breakdown processes that occur under specific initial conditions (Fox & Le Bissonnais, 1998). This could explain why positive correlations between aggregate stability and soil erodibility (Coote *et al.*, 1988), as well as negative correlations, have been reported (Bajracharya *et al.*, 1992).

To measure aggregate stability, Le Bissonnais (1996) proposed a method consisting of three treatments applied to 3–5 mm aggregates, that differentiate between the various mechanisms of breakdown: slaking due to fast wetting (treatment I), microcracking due

to slow wetting (treatment II) and mechanical breakdown by stirring of pre-wetted aggregates (treatment III). The results are expressed as the resulting fragment size distribution and as the mean weight diameter (MWD), which is the sum of the mass fraction remaining on each sieve after sieving, multiplied by the mean aperture of the adjacent sieves. De Noni *et al.* (2002) compared the results from different methods of aggregate stability measurements to erosion rates obtained on experimental parcels. The model correlation coefficients were as follows: $r = 0.90$ for Le Bissonnais (1996); 0.76 for Yoder (1936); 0.72 for Kemper & Rosenau (1986); and 0.66 for Hénin *et al.* (1958). Amézketa et al. (1996) found equally good correlations between results from Le Bissonnais's method and splash erosion mass. In a recent paper, Le Bissonnais *et al.* (2002) showed that the three aggregate stability treatments allowed assessment of the spatial variation of aggregate stability at the field scale with respect to the topography, and determination of the seasonal variations in the structural behaviour of soil.

As described by Hairsine & Rose (1991), current conceptual models of interrill erosion consider three processes: (i) rainfall detachment, (ii) sediment deposition, and (iii) entrainment of sediment. Soil detachment is supposedly due to raindrop impacts, and the only role of shallow overland flow is to transfer downslope the detached aggregates (Kinnell, 1990; Hairsine *et al.*, 1999). At greater flow depth, the role of overland flow becomes more important and rill erosion can be initiated by detachment due to overland flow. Cohesive soil is considered to be composed of a number, n, of fragment size classes. The rate of rainfall detachment per unit area of soil, e, for sediment size class, i, is expressed as a power function of the rainfall rate, P, according to:

$$e_i = a_i P^p, \tag{1}$$

where a is the detachability of the original soil, p a non-dimensional exponent, and a is an empirical parameter, which is not based on physical measurements. Moreover, the process named "detachment" by Rose *et al.* (1983) regroups two sub-processes and can be

conceptually divided into the aggregate breakdown process, and the splash process which puts the resulting fragments in motion (Figure 1). Aggregate breakdown determines the size distribution of fragments available for mobilization by raindrop splash and then transported by splash and by overland flow. We propose, therefore, to use the fragment size distributions resulting from aggregate stability treatments, measured using the method of Le Bissonnais (1996), to express the aggregate breakdown dynamics.

This paper describes the investigation of the potential of aggregate stability measurements for the assessment and modelling of aggregate breakdown dynamics under rainfall. As aggregate stability is measured on various aggregate sizes depending on the method, four initial aggregate size classes: 0–3 mm, 3–5 mm, 5–10 mm and 10–20 mm have been used in order to test the influence of initial aggregate size on the size distribution of breakdown fragments. For each of these four initial aggregate size classes, two series of experiments were performed: (i) Aggregate Stability measurements (AS), and (ii) Aggregate Breakdown induced by rainfall measurements(AB) for comparison between the fragment size distribution obtained under rainfall simulation and from aggregate stability measurements.

Materials and methods

Soils

Samples were collected from the A horizons (upper 15 cm) of two cultivated soils (Alfisols), a silt loam and a clay loam. Clay content was 112 g kg^{-1} for the silt loam and 360 g kg^{-1} for the clay loam. The organic C content was 20 g kg^{-1} for the silt loam and 18 g kg^{-1} for the clay loam. The silt loam was formed from aeolian deposits of the western part of the Paris Basin (Normandy, France), which is a zone very sensitive to erosion. The clay loam was formed from a marly molasse of the Basin of Aquitaine (Lauragais, France). The silt loam was collected in April 2001, after ploughing to establish potato mono-culture, and the clay loam was collected in July 2001, after stubble ploughing following the wheat harvest. After removal from the field, both soils were air-dried and

sieved at 20 mm.

For both series of experiments, the soils were segregated into four initial aggregate size classes by dry sieving: < 3 mm, 3–5 mm, 5–10 mm, and 10–20 mm and aggregates were oven dried for 24 h at 40°C in order to limit moisture variations. Water content was 0.07 g kg^{-1} for the silt loam and 0.17 g kg^{-1} for the clay loam.

Aggregate stability measurements (AS)

The three aggregate stability treatments were applied to each of the four initial aggregate size classes, according to the method proposed by Le Bissonnais (1996) and tested by Amézketa et al. (1996), Le Bissonnais & Arrouays (1997), Le Bissonnais *et al.* (2002) and de Noni *et al.* (2002). In this method, three treatments are applied to aggregates in order to distinguish between mechanisms of breakdown: slaking due to fast-wetting (fast-wetting treatment), occurring, for example, during heavy storms on dry soils; micro-cracking due to slow-wetting (slow-wetting treatment), which may occur during low-intensity rain; and mechanical breakdown by the stirring of pre-wetted aggregates (stirring treatment), which corresponds to aggregate behaviour during continuously wet periods. Each treatment was replicated three times for each initial aggregate size class.

Aggregate breakdown induced by rainfall (AB)

Simulated rainfall with deionised water was applied at 30.3 mm h^{-1} (standard error = 1.2 mm h^{-1} and spatial variability < 5 %). The rainfall simulation device and its characteristics are described by Chaplot & Le Bissonnais (2000). The kinetic energy was 16.2 J mm^{-1} and the peak raindrop size was 1.5 mm. Three replicated rainfall simulations were performed for each initial aggregate size class for both soils. The rain duration was chosen from previous experiments performed on these soils using the same rainfall intensity and corresponded to the length of time before runoff begins, i.e. 40 minutes for the silt loam and 60 minutes for the clay loam (Leguédois & Le Bissonnais, 2004).

Experimental devices (Figure 2) were built with an inner ring to hold the aggregates

and a large ring to keep all the splashed fragments inside. Filter paper ensured sufficient infiltration, so that water was recovered for each device. Once weighed, we knew the exact cumulative rainfall amount for each device. As for the aggregate stability measurements, the experiments were performed on 5 g of aggregates. For each rainfall simulation and for each initial aggregate size class, nine devices with 5 g of aggregates were submitted to rainfall. The whole fragments produced by aggregate breakdown and splash were collected after receiving various rainfall amounts, so that we obtained nine samples with different levels of breakdown.

Fragment size distribution measurements

The fragment size measurements were performed after AS and AB experiments, for each treatment or rainfall duration and for each initial aggregate size class. Ethanol was used for collecting the fragments in order to preserve the structure of the whole fragments produced. The fragment size distributions were obtained by combining sieving and laser diffraction. Fragments up to 500 μm were sieved in ethanol at 2000, 1000, and 500 μm. Fragments smaller than 500 μm were analysed with a laser diffraction sizer as 12 fractions, from 0.05 μm to 500 μm. These 12 fractions corresponded to volume frequencies of the different size fractions. The four coarsest size fractions (>2000 μm, 1000–2000 μm, 500–1000 μm, and < 500 μm) were then collected and oven dried at 105°C to obtain their masses. The calculation of the size distribution, including 16 size fractions, was made by combining the volume frequencies obtained with the laser diffraction sizer with the masses of the different size fractions. For this calculation, it was assumed that the bulk density of the different size fractions was similar. Then, fragment size distributions were expressed using the Mean Weight Diameter (MWD), which is the sum of the mass percentage of each size fraction multiplied by the mean size of the fraction (Kemper & Rosenau, 1986).

Statistical analysis

An overall test of coincidence of two non-linear regressions was made to assess if two data sets were significantly different. The two data sets correspond to the MWDs obtained for various cumulative rainfalls applied to two distinct initial aggregate size classes. The objective was to test the hypothesis, H_0, that two regression curves are similar. The principle of this test was the comparison of the residual variability obtained with only one model to the residual variability obtained with two distinct models fitted for each set of experimental data. For this, the two data sets were fitted with two distinct power functions of the rainfall variable and the residual variability $S^2_{y\,x_a}$ for both fits was calculated. The same was done by fitting a unique model to both data sets and $S^2_{y\,x_b}$ was calculated. Then the quality of the fitting was calculated by:

$$S^2_{y\,x_c} = ((n_1 + n_2 - 2)\, S^2_{y\,x_b} - (n_1 + n_2 - 4)\, S^2_{y\,x_a})\ /\ 2, \tag{2}$$

where n_1 and n_2 are the number of calculated values for each of the two aggregate size classes. Lastly, we quantified the relative improvement by two distinct models against one by calculating the F value of the Fischer-Snedecor test:

$$F = S^2_{y\,x_c}\ /\ S^2_{y\,x_a}. \tag{3}$$

If $F > F^2_{n_1+n_2-4}$, H_0 was rejected, meaning that a significantly better fit was obtained by considering two distinct models.

Results

Influence of the initial aggregate size class on the fragment size distribution resulting from AS

The analysis of Mean Weight Diameters, calculated, respectively, with (Figure 3(a)) and without (Figure 3(b)) the > 2000 μm size fraction, shows the difference in aggregate stability between both soils for the three treatments. It shows the higher stability of the clay loam. A noticeable point is that, for the three treatments, the MWD increases as

the size of initial aggregates increases. The fragment size distribution analysis of the four initial aggregate size classes shows that the greatest diffference is observed for the largest > 2000 μm fraction (Figure 4). For the clay loam, the MWDs calculated without the > 2000 μm fraction for the slow-wetting and stirring treatments are not significantly different for the four initial aggregate size classes, except for the slow-wetting treatment applied to 3–5 mm aggregates (Figure 3(b)). For the silt loam, the comparison between the MWDs calculated without the > 2000 μm fraction for the three treatments shows that only the < 3 mm size class is significantly different from the other initial aggregate size class (Figure 3(b)). These results show that the variation in the MWDs between initial aggregate size classes are partly due to the effect of the > 2000 μm fraction. In fact, complete aggregate breakdown is not instantaneous. Increasing rainfall duration is probably required to reach complete breakdown when the size of initial aggregates increases (Le Bissonnais, 1988) and when clay content increases.

For both soils, the lowest MWD is obtained for the fast-wetting treatment applied to the smallest size of initial aggregates (< 3 mm). The fast-wetting treatment is also the most destructive whatever the initial aggregate size. In addition, this treatment differs from the two others because, even if we calculate the MWD without the > 2000 μm fraction (Figure 3), the MWD increases when the size of initial aggregates increases.

For the three treatments performed on the silt loam, the fragment size distribution analysis shows a bimodal frequency curve with two modes: one around 750 μm and the other one around 75 μm (Figure 5a). For the clay loam (Figure 5b), the 75 μm peak almost vanished, but another one is visible around the > 2000 μm fraction. The clay loam produces coarser fragments than the silt loam.

Compared to the other treatments, the fast-wetting treatment generated the greatest amount of aggregates from 50 to 500 μm. Aggregates resulting from breakdown were coarser for the clay loam than for the silt loam. The slow-wetting treatment produced the smallest quantity of fine fragments. The stirring treatment generated the greatest

quantity of fine fragments < 50 μm. These fragments result from the abrasion of the periphery of aggregates due to the mechanical energy applied during the treatment. This is a cumulative process and the quantity of fine fragments (< 50 μm) is proportional to the duration of the mechanical energy (Le Bissonnais, 1988).

The differences observed in the MWDs analysis between both soils result from differences in the intensity of the breakdown mechanisms, especially due to clay content (Le Bissonnais, 1988). For slow-wetting and stirring treatments, the same fragment size distributions resulting from aggregate breakdown is found, irrespective of the initial aggregate size class, particularly for the clay loam (Figure 3(b)). These fragment size distributions resulting from aggregate breakdown could be considered as characteristic signatures of soils, and related to an elementary fabric of the material.

Dynamics of aggregate breakdown under rainfall simulation (AB)

As we obtained fragment size distributions for increasing cumulative rainfall values, the dynamics of aggregate breakdown were analyzed by calculating an indicator of the MWD decrease. Each value of the indicator corresponds to the difference between the MWD before a rainfall simulation and the MWD at x mm of cumulative rainfall divided by x. We obtained the aggregate breakdown kinetics based on the mean decrease of the MWD for 1 mm of rainfall. These kinetics are similar for both soils (Figure 6), with two different stages during a rainfall event. The first is named "quasi-instantaneous" aggregate breakdown because of the rapid decrease of the MWDs. This rapid stage is particularly present for the silt loam, where the MWD of 3–5 mm aggregates decreases from 3500 μm to 980 μm under 3 mm of rainfall. It corresponds to a 70 % decrease of the MWD value for all the initial aggregate size classes of the silt loam. There is only a 40 % decrease for the clay loam. After 5 mm of rainfall, the second stage shows a slower decrease of the MWDs. During this last stage, the MWDs decrease for the silt loam is twice that of the clay loam.

As for the analysis of aggregate stability measurements, the MWDs have been calcu-

lated without the > 2000 μm fraction (Figure 7). For the silt loam, the MWD of the fragments resulting from aggregate breakdown is higher for larger initial aggregates. For the clay loam, only the MWD of the < 3 mm class seems to be smaller than the three other classes. Statistical tests of regression coincidence were performed to determine if the models fitted for each of the four initial size classes (Figure 7) were significantly different. The comparisons have been made for the couples of initial aggregate size class with close tendancy curves. It shows that each initial aggregate size class has different breakdown dynamics, except for both largest classes of the clay loam (Table 1). The computation of the ratio $F \ / \ F^2_{n_1+n_2-4}$ enabled us to evaluate the sensitivity of the statistics. This ratio is close to one for the three largest initial aggregate size classes of the clay loam. It shows that the difference between classes of the MWD decrease is much more marked for the silt loam than for the clay loam.

For both soils, the analysis of the dynamics of each fraction resulting from aggregate breakdown can be described by a power function of the cumulative rainfall variable. We can distinguish three size ranges with a specific dynamics (Figure 8(a)):

1. > 2000 μm: The mass percentage of this size range decreases rapidly during the first three millimetres of rainfall.

2. 250–2000 μm: During the first three millimetres of rainfall, the mass percentage of fragments increases due to the breakdown of > 2000 μm aggregates. Then, this quantity decreases because the aggregates are themselves broken down into finer aggregates; after three millimetres of rainfall there are few > 2000 μm aggregates remaining to be broken down into 250–2000 μm fragments.

3. < 250 μm: This size range grows because of the progressive breakdown of > 250 μm aggregates into < 250 μm fragments. This size range could correspond to the panel of elementary micro-aggregates which are put together to form the > 250 μm macro-aggregates.

Discussion

Comparison between AB and AS: initial aggregate size class and breakdown mechanisms

The behaviour of each soil and aggregate size class under rainfall simulation is in agreement with the results of aggregate stability measurements. For the rainfall experiment applied to the silt loam, the MWDs calculated without the > 2000 µm fraction are greater when the size of initial aggregates is larger. This relationship is less marked for the clay loam (Figure 7). We can explain this response, depending on the initial aggregate size, by considering the mechanism of micro-cracking. Micro-cracking is the result of two different mechanisms with different physical processes: differential swelling and partial slaking (Le Bissonnais, 1996). Both processes produce micro-aggregates of the same size and type but they occur in soil with different clay content (Chan & Mullins, 1994): as the clay content increases, partial slaking decreases and breakdown by differential swelling increases. Partial slaking is directly related to the wetting stage in the presence of air, and is particularly intense when the porosity is bigger and also when the clay content is small (Le Bissonnais, 1988). For the silt loam, we inferred that micro-cracking is the result of breakdown by partial slaking. As with the slaking mechanism, partial slaking is caused by the compression of air entrapped inside aggregates but at a smaller rate. Because of a bigger porosity in the silt loam and a sufficient rainfall rate, air can be trapped. For the silt loam, it explains why we obtain a gradual response for each initial aggregate size similar to the response to the fast-wetting treatment.

Furthermore, considering the rapid MWD decrease of the < 3 mm class for both soils (Figure 6), we can say that our rainfall simulation is destructive for the finest aggregates regardless of the soil aggregate stability. According to Le Bissonnais (1988), the finest aggregates are the most vulnerable because the ratio between the rainfall intensity and the pore volume is large. In our experiment, the mode of the raindrop size distribution produced by the simulator is 1.5 mm diameter (78 % of the volume of rainfall corresponds to raindrops from 1 to 2 mm). The MWD of the < 3 mm class before rainfall is 1.3 mm for the silt loam and 1.4 mm for the clay loam. For both soils, the ratio *raindrop size : initial*

aggregate size is close to one. For < 3 mm aggregates, our rainfall conditions are close to those of the fast-wetting treatment. That is the reason why slaking is more prevalent in the < 3 mm aggregate size class than in the other classes. It explains why the MWDs for the < 3 mm size class (Figure 7) are so small and why their decrease is so rapid (Figure 6).

To explain the greater resistance of the largest aggregates, we hypothesise that the clay content and/or the organic matter content increases as the aggregate size increases. During sieving, the silt loam produced a very small quantity of 10-20 mm aggregates. The 10-20 mm aggregates we obtained were probably high in organic matter and in clay content, which possibly explains their "survival". In many studies, stable macro-aggregates of cultivated soils are often enriched in total C as compared to soil micro-aggregates (Puget *et al.*, 1995) and in particulate organic matter (Cambardella & Elliott, 1993; Puget *et al.*, 2000). Considering the clay content, Puget *et al.* (2000) found that water-stable macroaggregates were not enriched in clay or silt when compared to microaggregates, the converse of the Dormaar (1983) study. To verify these hypotheses, it is necessary to measure and characterise the organic matter and clay contents contained in the aggregates of each initial aggregate class.

Regarding the global pattern of the fragment size distributions, we observed a relative independence of the fragment size distributions resulting from breakdown from initial aggregate size (Figure 4). In the resulting fragment size distributions, the relative importance of each mode varies in relation to the clay content. As described by Le Bissonnais (1988), clay content seems to explain differences in the MWDs of both soils. As the duration of the energy applied is the same for all initial aggregate sizes, and considering that breakdown occurs progressively from the periphery to the centre of aggregates (Le Bissonnais, 1988), it is logical to obtain a greater MWD for the coarsest initial aggregate classes, even if the MWD is expressed without the > 2000 µm fraction.

Comparison between AB and AS: temporal dynamics of breakdown mechanisms

The fast-wetting treatment is more destructive than the rainfall applied in the AB exper-

iments. For both soils, the size distribution of fragments produced quasi-instantaneously with the fast-wetting treatment is very different from the one obtained during the first millimetres of rainfall. Slaking, which is responsible for aggregate breakdown in the fast-wetting treatment, occurs on dried aggregates (Le Bissonnais, 1988). Thus this mechanism could only happen during the first millimetres of rainfall, which is not the case.

The clay loam yielded almost the same response for all initial aggregate size classes submitted to rainfall. This confirms that slaking is not dominant under our rainfall conditions. If it were, the MWD of the four initial size classes obtained under rainfall would be different from each other, as it is so for the fast-wetting treatment. Therefore, we can conclude that the breakdown we observe under rainfall simulation corresponds to the cumulative effect of microcracking and mechanical breakdown mechanisms. These mechanisms are simulated by the slow-wetting treatment and the stirring treatment, respectively.

As we can see for the 3–5 mm aggregates of the silt loam (Figure 8), the fragment size distribution resulting from the slow-wetting treatment is similar to the fragment size distribution obtained after 3.2 mm of rainfall. During the first three millimetres of rainfall, the microcracking mechanism is also predominant and its intensity seems to be at a maximum at about 3 mm of cumulative rainfall. The fragment size distribution obtained for the stirring treatment, enriched in fine fragments around the 75 µm peak, which is typical of this treatment, is similar to the fragment size distribution obtained after 21.2 mm of rainfall.

Mechanical breakdown due to raindrop impact is an important process for wet soils because the aggregates are weaker (Le Bissonnais, 1996). The breakdown is proportional to the duration of the mechanical energy applied (Le Bissonnais, 1988). We observed differences in the quantities of fine fragments (about 75 µm) produced between the four initial aggregate size classes. For both soils, comparing the fragment size distribution obtained at the end of the rainfall simulation to the fragment size distribution obtained from the stirring treatment, we observed that the < 3 mm aggregate class produces more fine

fragments under rainfall than during the stirring treatment. This tendency is reversed for the 10–20 mm class. For the 3–5 mm class, size distributions are similar for the stirring treatment and the rainfall simulation. This means that the mechanical energy applied during the stirring treatment is equivalent to the effect of 30 mm of rainfall at 30 mm h^{-1}. This also shows that the raindrop effect is particularly important and rapid when the size of the aggregates is small. During the stirring treatment, the aggregates receive mechanical energy once they are completely wet. The difference between AB and AS experiments is, that under rainfall simulation, the wetting is more progressive than during the stirring test. The saturation of large aggregates under rainfall is particularly slow.

Relation between aggregate structural organisation and aggregate breakdown

Regarding the dynamics of each of the 16 fragment size fractions resulting from breakdown, the mass percentage of the whole < 250 µm size fractions increases during rainfall (Figure 8). This means that the > 250 µm aggregates are progressively broken down into < 250 µm aggregates. Our results confirm those of Tisdall & Oades (1982), Oades & Waters (1991), and Puget *et al.* (2000), who proposed a hierarchical model of soil aggregation in which macroaggregates are made by the binding together of microaggregates. We can assume a very simple hierarchical organisation at two levels for aggregates of ploughed layers of cultivated soils: microaggregates (< 250 µm) are brought together in macroaggregates (Plante *et al.*, 2002) and progressively separated during breakdown (Figure 9).

In our case, aggregate breakdown results from physical mechanisms. Aggregates have pores of different sizes, which determine the distribution and strength of failure zones (Perfect & Kay, 1991). Physical breakdown mechanisms occur at the weakest points of aggregate structure. For a given energy input, the probability of aggregate failure increases with increasing aggregate size (Marshall & Quirk, 1950; Coughlan *et al.*, 1973). For both soils, we obtained a continuous enrichment in < 250 µm aggregates during rainfall. We conclude that the aggregate structure of both soils is made by the binding together

of < 250 μm aggregates. We also consider that the energy applied during our rainfall simulations corresponds to the energy required to break down coarse aggregates in < 250 μm aggregates, but is not sufficient to break down these 250 μm aggregates into smaller units.

Modelling soil detachment dynamics using aggregate stability measurements

The hierarchical model of soil aggregation allows categorisation of the dynamics of 16 size fractions into two size ranges. The > 250 μm size range, whose total mass percentage decreases during rainfall, P, includes the four coarsest fractions, j. This total mass percentage can be written as $\sum B_j$ with $j = 1, 2 \ldots 4$. The total mass percentage corresponding to the < 250 μm size range, with the finest size fractions, k, can be written as $\sum B_k$ with $k = 5, 6 \ldots 16$, with B_k increasing during rainfall. The conservation of sediment mass percentage in fragment size fractions j and k can be written as:

$$\sum_{1}^{4} B_j(P) + \sum_{5}^{16} B_k(P) = 1. \tag{4}$$

Considering that the three mechanisms (slaking, microcracking, and mechanical breakdown) reproduced by the three aggregate stability treatments are dominant at different times during a rainfall event (Figure 10), we propose equation (5), which gives the mass percentage, B_i, of fragments of each of the 16 size fractions, i, available at P millimetres of cumulative rainfall:

$$B_i(P) = \alpha\,[\text{Fast-wetting}]_i\,(P) + \beta\,[\text{Slow-wetting}]_i\,(P) + \chi\,[\text{Stirring}]_i\,(P), \tag{5}$$

where α, β, and χ are constants.

Results obtained for aggregate stability measurements showed that the fast-wetting treatment was more destructive than that observed during the rainfall experiment. This means that the fragment size distributions obtained from the fast-wetting treatment do not correspond to the size distribution of fragments resulting from aggregate breakdown under

a 30 mm h^{-1} rainfall rate (Figure 8). For greater rainfall intensities, the slaking process, which is simulated by the fast-wetting treatment, would probably be present and dominant during the first millimetres of rainfall (Concaret, 1967). In this case, the use of the fast-wetting treatment variable would better describe the fragment size distribution obtained under rainfall. This would also be true for larger raindrops such as those observed during heavy storms. In our case, the dynamics of soil detachment are modelled without the fast-wetting term of equation (5), using only the slow-wetting and stirring treatments, as represented in Figure 6. Dynamics are modelled with power functions of the rainfall variable as:

$$B_i(P) = [\text{Slow-wetting}]_i \, m \, P^n + [\text{Stirring}]_i \, r \, P^s, \tag{6}$$

where $[\text{Slow-wetting}]_i$ and $[\text{Stirring}]_i$ are the percentage of the fraction i obtained for each aggregate stability treatment, P the cumulative rainfall, m, n, r and s are constants characteristic of each soil.

As the fragment size distributions resulting from breakdown are qualitatively independent from the size of initial aggregates, non-linear regression was made for the breakdown of 3–5 mm aggregates. This modelling consists of fitting the measured percentage to equation (6), which is based on the mass percentage of each of the 16 size fractions measured from aggregate stability treatments. The values of the m, n, r and s parameters have been optimised for each soil by minimising the distance:

$$\sum_{i=1}^{16} \left(B_i \exp(P) - B_i \bmod(P) \right)^2 , \tag{7}$$

with B_i exp the experimental value of the mass percentage of a fraction i, and $B_i$mod, the predicted value of the mass percentage of a fraction i. The optimisation of m, n, r and s parameters was made on a data set corresponding to one replicate, the model obtained from which ($n = 135$), was then used to predict the mass percentage of the validation set corresponding to the two other replicates ($n = 270$). We obtained excellent coefficients of correlation for both soils (r=0.87 for the soilt loam and r=0.91 for the clay

loam), as presented for the silt loam in Figure 11. These first results show it is possible to express the aggregate breakdown,B_i,on the basis of aggregate stability measurements. It makes it possible to know the size distribution of fragments available to be put in motion by raindrop impacts and then transported by splash or runoff (Figure 1) for various cumulative rainfall values, from the fragment size distribution obtained with the aggregate stability measurements. In equation (6), the dynamics are modelled with the rainfall variable in terms of cumulative rainfall and, so, it doesn't take the rainfall intensity into account. The rainfall energy, coupling cumulative rainfall and rainfall intensity, would certainly describe the aggregate breakdown dynamics more generally. The relevance of the fast-wetting treatment in soil detachment modelling has to be tested for greater rainfall intensities. It would be interesting to determine ranges of rainfall rate where combinations of the three aggregate stability treatments describe correctly the fragment size distribution dynamics of breakdown products. Complementary experiments could also be performed on other types of soils in order to assess the validity range of this model. Variables such as clay content could certainly be used to explain the differences in the parameter values between both soils (Meyer & Harmon, 1984).

Conclusions

The aim of this study was to investigate the potential of aggregate stability measurements for the assessment and modelling of aggregate breakdown dynamics under rainfall which is the first step of the interrill erosion process.

We showed that the fragment size distribution resulting from breakdown were very similar for the four initial aggregate size class, indicating that the same mechanisms were involved. The differences observed from one class to another resulted essentially from the duration of these mechanisms while the differences between soils were in terms of the intensity of the breakdown mechanisms.

Another result was that the fragment size distributions obtained with the aggregate stability measurements were similar to those obtained under rainfall experiments. The

gradual response obtained for various cumulative rainfall values was due to the relative magnitude of the different physical mechanisms simulated by the three aggregate stability treatments.

We have identified a similar structural organisation of aggregates from ploughed layers for the clay loam and the silt loam. The macroaggregates are constructed from < 250 μm microaggregates, which progressively detach at the weakest point of the aggregate structure under rainfall action.

These results allowed modelling of the dynamics of aggregate breakdown under rainfall on the basis of the fragment size distributions resulting from aggregate stability measurements. This aggregate breakdown model could be combined with temporal data or models of fragment size distributions of splashed fragments and sediments transported by overland flow. This should enable the evaluation of the size selectivity of the mobilisation and transport processes, and development of a global model of sediment transfer in interrill erosion.

Acknowledgements

The authors appreciate the skilled assistance of B. Renaux and L. Prud'Homme for rainfall simulations, H. Gaillard for aggregate stability measurements, F. Darboux for scientific discussions, and K. Wein and T. Ellis for English language corrections.

References

Amézketa, E., Singer, M. J., and Le Bissonnais, Y. (1996). Testing a new procedure for measuring water-stable aggregation. *Soil Science Society of America Journal*, 60(3):888–894.

Bajracharya, R. M., Elliot, W. J., and Lal, R. (1992). Interrill erodibility of some Ohio

soils based on field rainfall simulations. *Soil Science Society of Amercia Journal*, 56(1):267–272.

Bradford, J. M., Ferris, J. E., and Remley, P. A. (1987). Interrill soil erosion processes: II. Relationship of splash detachment to soil properties. *Soil Science Society of America Journal*, 51(6):1571–1575.

Cambardella, C. A. and Elliott, E. T. (1993). Carbon and nitrogen dynamics of soil organic matter fractions from cultivated and native grassland soils. *Soil Science Society of America Journal*, 57(4):1071–1076.

Chan, K. Y. and Mullins, C. E. (1994). Slaking characteristics of some Australian and British soils. *European Journal of Soil Science*, 45:273–283.

Chaplot, V. and Le Bissonnais, Y. (2000). Field measurements of interill erosion under different slopes and plot sizes. *Earth Surface Processes and Landforms*, 25:145–153.

Concaret, J. (1967). Étude des mécanismes de la destruction des agrégats de terre au contact de solutions aqueuses (2). *Annales agronomiques*, 18(2):99–144.

Coote, D. R., Malcolm-McGovern, C. A., Wall, G. J., Dickinson, W. T., and Rudra, R. P. (1988). Seasonal variation of erodibility indices based on shear strength and aggregate stability in some Ontario soils. *Canadian Journal of Soil Science*, 68:405–416.

Coughlan, K. J., Fox, W. E., and Hughes, J. D. (1973). Aggregation in swelling clay soils. *Australian Journal of Soil Research*, 11:133–141.

de Noni, G., Blavet, D., Laurent, J.-Y., Le Bissonnais, Y., and Asseline, J. (2002). Proposal of soil indicators for spatial analysis of carbon stocks evolution. In *17th World Congress of Soil Science*, page 13, Bangkok, Thailande. Paper n°30, Symposium 35.

Dormaar, J. F. (1983). Chemical properties of soil and water-stable aggregates after sixty-seven years of cropping to spring wheat. *Plant and Soil*, 75:51–61.

Emerson, W. W. (1967). A classification of soil aggregates based on their coherence in water. *Australian Journal of Soil Research*, 5:47–57.

Fox, D. M. and Le Bissonnais, Y. (1998). Process-based analysis of aggregate stability effects on sealing, infiltration, and interrill erosion. *Soil Science Society of America Journal*, 62(3):717–724.

Hairsine, P. B. and Hook, R. A. (1994). Relating soil erosion by water to the nature of the soil surface. In So, H. B., Smith, G. D., Raine, S. R., Schafer, B. M., and Loch, R. J., editors, *Sealing, Crusting and Hardsetting Soils: Productivity and Conservation*, pages 77–91, University of Queensland, Brisbane, Australia. Second International Symposium on Sealing, Crusting and Hardsetting Soils: Productivity and Conservation, Australian Society of Soil Science Inc. and ISSCHS.

Hairsine, P. B. and Rose, C. W. (1991). Rainfall detachment and deposition: Sediment transport in the absence of flow-driven processes. *Soil Science Society of America Journal*, 55(2):320–324.

Hairsine, P. B., Sander, G. C., Rose, C. W., Parlange, J.-Y., Hogarth, W. L., Lisle, I., and Rouhipour, H. (1999). Unsteady soil erosion due to rainfall impact: A model of sediment sorting on the hillslope. *Journal of Hydrology*, 220(3–4):115–128.

Haynes, R. J. (1993). Effect of sample pretreatment on aggregate stability measured by wet sieving or turbidimetry on soils of different cropping history. *Journal of Soil Science*, 44:261–270.

Hénin, S., Monnier, G., and Combeau, A. (1958). Méthode pour l'étude de la stabilité structurale des sols. *Annales Agronomiques*, 9(1):71–90.

Kemper, W. D. and Rosenau, R. C. (1986). Aggregate stability and size distribution. In Klute, A., editor, *Methods of soil analysis. Part 1. Physical and mineralogical methods*, volume 9 of *Agronomy Monograph*, pages 425–442. American Society of Agronomy, Soil Science Society of America, Madison, 2nd edition.

Kinnell, P. I. A. (1990). The mechanics of raindrop-induced flow transport. *Australian Journal of Soil Research*, 28:497–516.

Le Bissonnais, Y. (1988). *Analyse des mécanismes de désagrégation et de mobilisation des particules de terre sous l'action des pluies*. PhD thesis, Université d'Orléans, France.

Le Bissonnais, Y. (1996). Aggregate stability and assessment of soil crustability and erodibility: I. Theory and methodology. *European Journal of Soil Science*, 47:425–437.

Le Bissonnais, Y. and Arrouays, D. (1997). Aggregate stability and assessment of soil crustability and erodibility: II. Application to humic loamy soils with various organic carbon contents. *European Journal of Soil Science*, 48(1):39–48.

Le Bissonnais, Y., Cros-Cayot, S., and Gascuel-Odoux, C. (2002). Topographic dependance of aggregate stability, overland flow and sediment transport. *Agronomie*, 22:489–501.

Le Bissonnais, Y. and Singer, M. J. (1993). Seal formation, runoff and interrill erosion from 17 California soils. *Soil Science Society of America Journal*, 57:224–229.

Marshall, T. J. and Quirk, J. P. (1950). Stability of structural aggregates of dry soil. *Australian Journal of Agricultural Science*, 1:266–275.

Meyer, L. D. and Harmon, W. C. (1984). Susceptibility of agricultural soils to interrill erosion. *Soil Science Society of America Journal*, 48(5):1152–1157.

Oades, J. M. and Waters, A. G. (1991). Aggregate hierarchy in soils. *Australian Journal of Soil Research*, 29:815–828.

Perfect, E. and Kay, B. D. (1991). Fractal theory applied to soil aggregation. *Soil Science Society of America Journal*, 55(6):1552–1558.

Plante, A. F., Feng, Y., and McGill, W. B. (2002). A modelling approach to quantifying soil macroagregate dynamics. *Canadian Journal of Soil Science*, 82(2):181–190.

Puget, P., Chenu, C., and Balesdent, J. (1995). Total and young organic matter distributions in aggregates fo silty cultivated soils. *European Journal of Soil Science*, 46:449–459.

Puget, P., Chenu, C., and Balesdent, J. (2000). Dynamics of soil organic matter associated with particle-size fractions of water-stable aggregates. *European Journal of Soil Science*, 51(4):595–605.

Rose, C. W., Williams, J. R., Sander, G. C., and Barry, D. A. (1983). A mathematical model of soil erosion and deposition processes. I. Theory for a plane land element. *Soil Science Society of America Journal*, 47(5):991–995.

Tisdall, J. M. and Oades, J. M. (1982). Organic matter and water-stable aggregates in soils. *Journal of Soil Science*, 33:141–163.

Yoder, R. E. (1936). A direct method of aggregate analysis of soils and a study of the physical nature of erosion losses. *Journal of American Society of Agronomy*, 28(5):337–351.

List of Tables

1 Statistical ratios between calculated and theoretical values of the F-test at $P < 0.05$ for each couple of initial aggregate size class compared to each other. If $F > F^2_{n_1+n_2-4}$, the two data sets are significantly different. 25

F / $F^2_{n_1+n_2-4}$	< 3 mm compared to 3-5 mm	3-5 mm compared to 5-10 mm	5-10 mm compared to 10-20 mm	3-5 mm compared to 10-20 mm
Clay loam	11.12	1.85	0.09	1.22
Silt loam	18.58	5.47	14.23	33.82

Table 1

List of Figures

Fig. 1 Conceptual modelling of interrill erosion as three sub-processes: breakdown, mobilisation and transport/sedimentation. Initial aggregates (a) break down into fragments (b). Raindrops mobilise fine fragments (c), available for transport by overland flow for the finest (d) or sedimentation for the coarsest (e).

Fig. 2 Aggregate breakdown holder and collector.

Fig. 3 Aggregate stability measurements expressed as Mean Weight Diameters (MWD) computed for each fraction (a) and without the > 2000 μm fraction (b). Str: stirring treatment; SW: slow-wetting treatment; FW: fast-wetting treatment. Bars are standard errors. MWD values followed by a different lowercase letter within the same treatment and between the four initial aggregate size classes are significantly different at $P < 0.05$. Values followed by * within the same initial aggregate size class and between treatments are significantly different at $P < 0.05$.

Fig. 4 Fragment size distribution resulting from the fast-wetting treatment performed on the clay loam aggregates. Bars are standard errors.

Fig. 5 Fragment size distributions resulting from the three aggregate stability treatments on 3–5 mm initial aggregates for (a) the silt loam and (b) the clay loam. Bars are standard errors.

Fig. 6 MWD decrease indicators during rainfall simulation for each initial aggregate size, corresponding to the decrease of the MWD at each millimetre of rainfall for (a) the silt loam and (b) the clay loam. Curves are power functions of the cumulative rainfall.

Fig. 7 Dynamics of the MWDs resulting from breakdown under rainfall for (a) the silt loam and (b) the clay loam. The MWDs are calculated without the > 2000 μm fraction. Curves are power functions of the cumulative rainfall variable.

Fig. 8 Fragment size distribution resulting from breakdown of 3–5 mm aggregates for the silt loam. Comparison between size distribution of breakdown products resulting from various cumulative rainfall heights (a) and aggregate stability measurements (b). Bars are standard errors (b).

Fig. 9 Relationship between aggregate breakdown and aggregate structural organisation of ploughed layers of cultivated soils.

Fig. 10 Theoretical schemas for the organisation and evolution of aggregate breakdown mechanisms, where (a) represents the supposed predominance of each of the three physical mechanisms responsible for breakdown at specific moments of a rainfall event, (b) corresponds to the simplified schema of what we really observe during the rainfall simulations at 30 mm h^{-1}.

Fig. 11 Comparison of the modelled mass percentage of breakdown fragments vs measurements, for 3–5 mm aggregates of the silt loam and for various cumulative rainfall values.

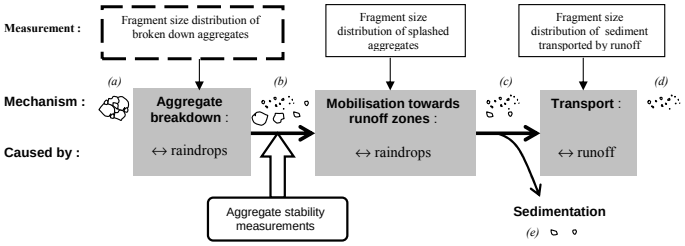
Measurement :
Fragment size distribution of broken down aggregates
Fragment size distribution of splashed aggregates
Fragment size distribution of sediment transported by runoff
(a)
(b)
(c)
(d)
Mechanism :
Caused by :
Aggregate breakdown :
↔ raindrops
Mobilisation towards runoff zones :
↔ raindrops
Transport :
↔ runoff
Aggregate stability measurements
Sedimentation
(e)

Figure 1

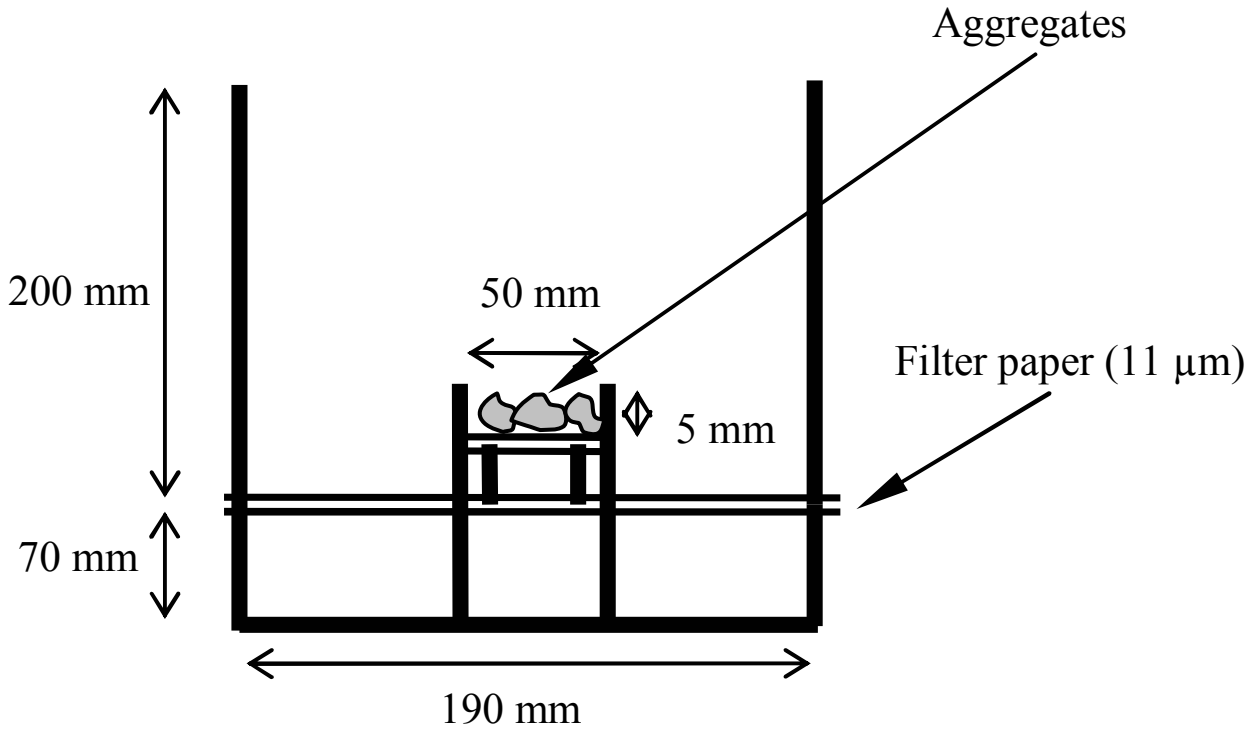

Figure 2

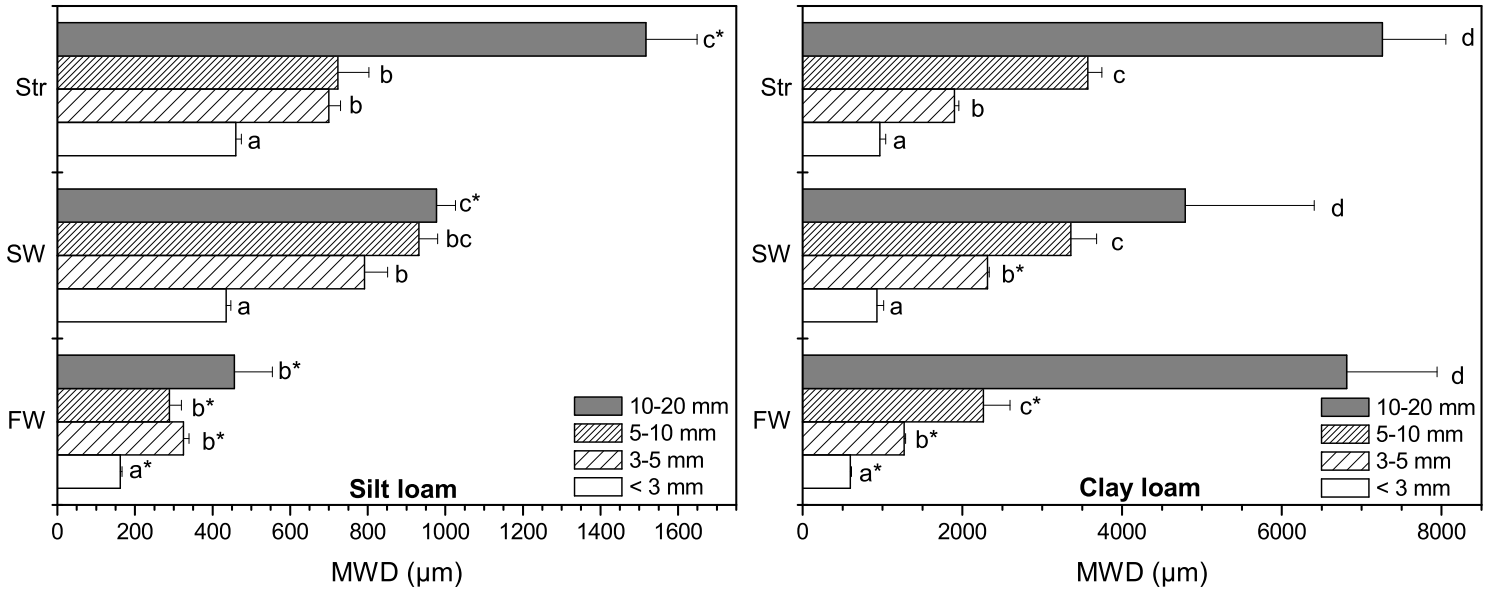
Str
SW
FW
c*
b
b
a
c*
bc
b
a
b*
b*
b*
a*
10-20 mm
5-10 mm
3-5 mm
< 3 mm
Silt loam
0
200
400
600
800
1000
1200
1400
1600
MWD (μm)
d
c
b
a
d
c
b*
a
d
c*
b*
a*
Clay loam
0
2000
4000
6000
8000
MWD (μm)

(a)

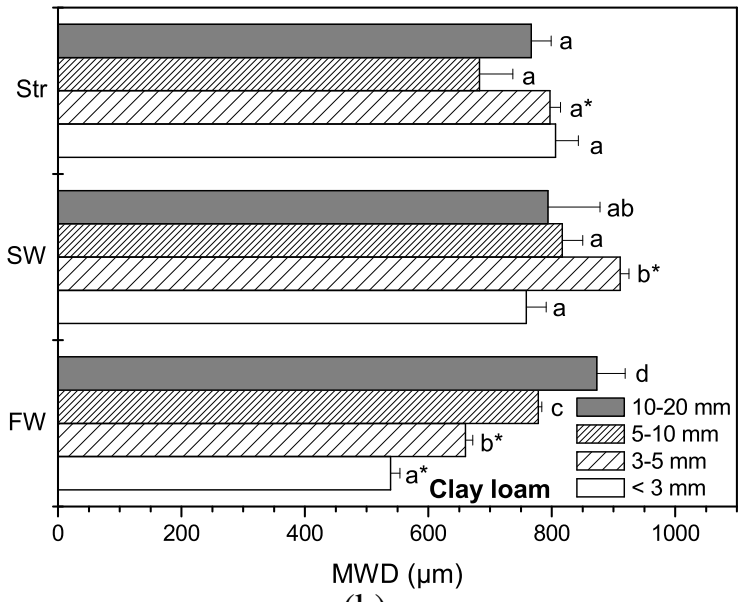
Str
SW
FW
a
a
a*
a
ab
a
b*
a
d
c
b*
a*
10-20 mm
5-10 mm
3-5 mm
< 3 mm
Clay loam
0
200
400
600
800
1000
MWD (μm)

(b)

Figure 3

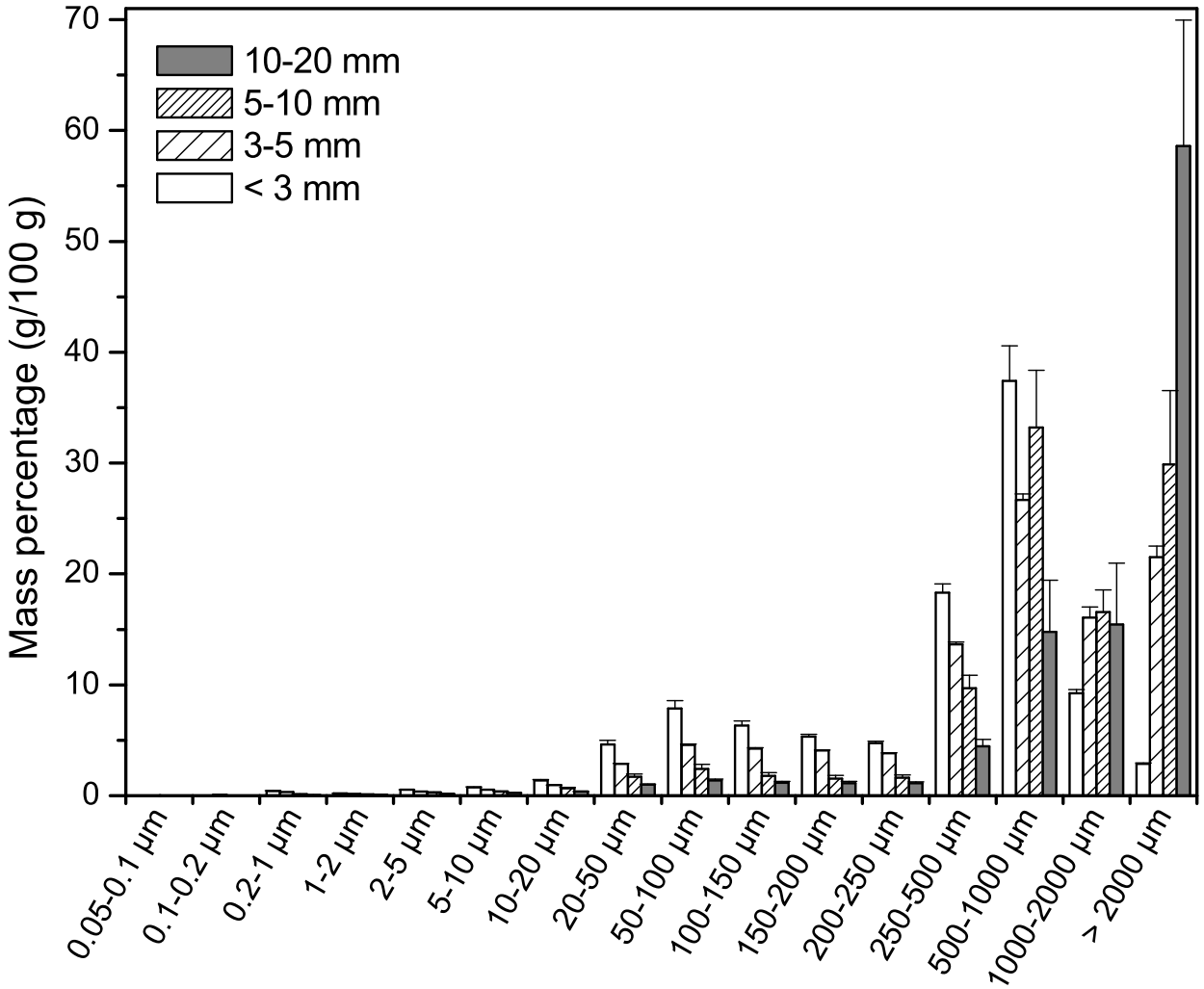
10-20 mm
5-10 mm
3-5 mm
< 3 mm
Mass percentage (g/100 g)
0
10
20
30
40
50
60
70
0.05-0.1 µm
0.1-0.2 µm
0.2-1 µm
1-2 µm
2-5 µm
5-10 µm
10-20 µm
20-50 µm
50-100 µm
100-150 µm
150-200 µm
200-250 µm
250-500 µm
500-1000 µm
1000-2000 µm
> 2000 µm

Figure 4

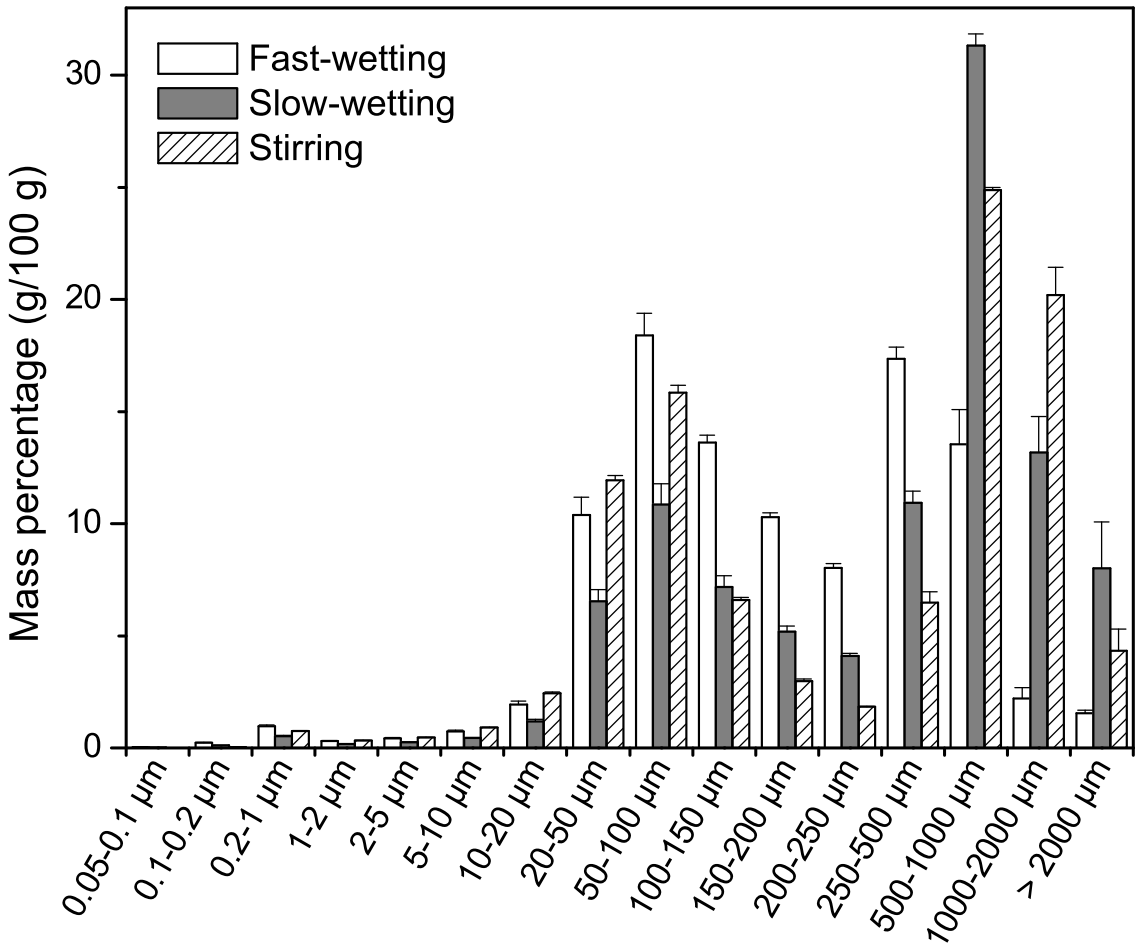
Fast-wetting
Slow-wetting
Stirring
Mass percentage (g/100 g)
0
10
20
30
0.05-0.1 μm
0.1-0.2 μm
0.2-1 μm
1-2 μm
2-5 μm
5-10 μm
10-20 μm
20-50 μm
50-100 μm
100-150 μm
150-200 μm
200-250 μm
250-500 μm
500-1000 μm
1000-2000 μm
> 2000 μm

(a)

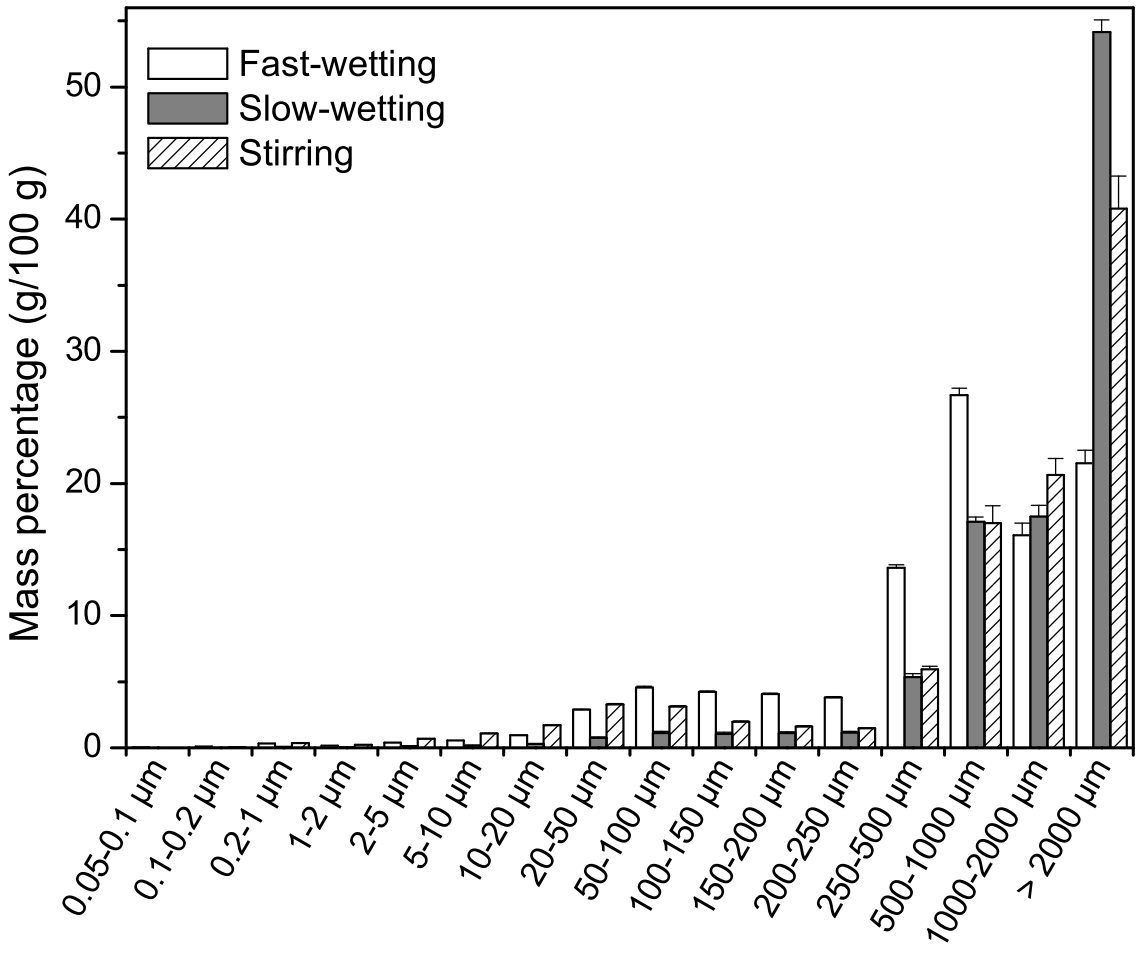
Fast-wetting
Slow-wetting
Stirring
Mass percentage (g/100 g)
0
10
20
30
40
50
0.05-0.1 μm
0.1-0.2 μm
0.2-1 μm
1-2 μm
2-5 μm
5-10 μm
10-20 μm
20-50 μm
50-100 μm
100-150 μm
150-200 μm
200-250 μm
250-500 μm
500-1000 μm
1000-2000 μm
> 2000 μm

(b)

Figure 5

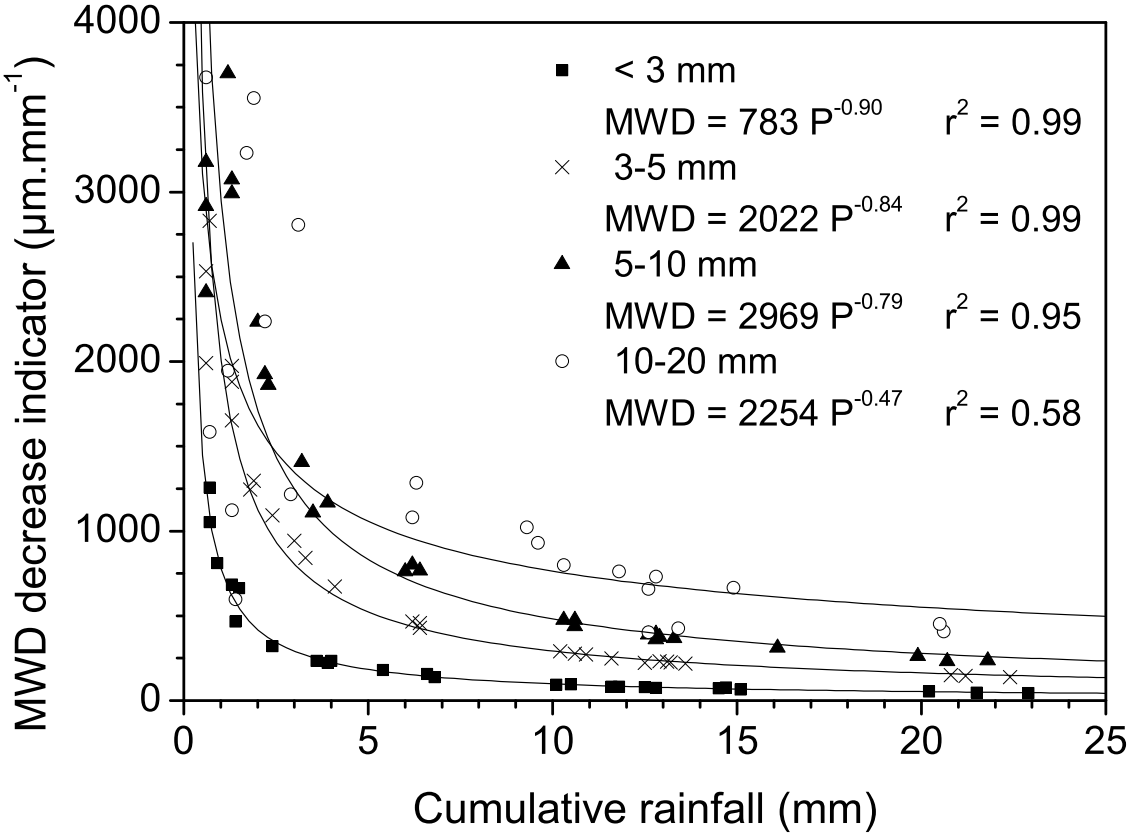
MWD decrease indicator (µm.mm-1)
Cumulative rainfall (mm)
< 3 mm
MWD = 783 P-0.90 r2 = 0.99
3-5 mm
MWD = 2022 P-0.84 r2 = 0.99
5-10 mm
MWD = 2969 P-0.79 r2 = 0.95
10-20 mm
MWD = 2254 P-0.47 r2 = 0.58

(a)

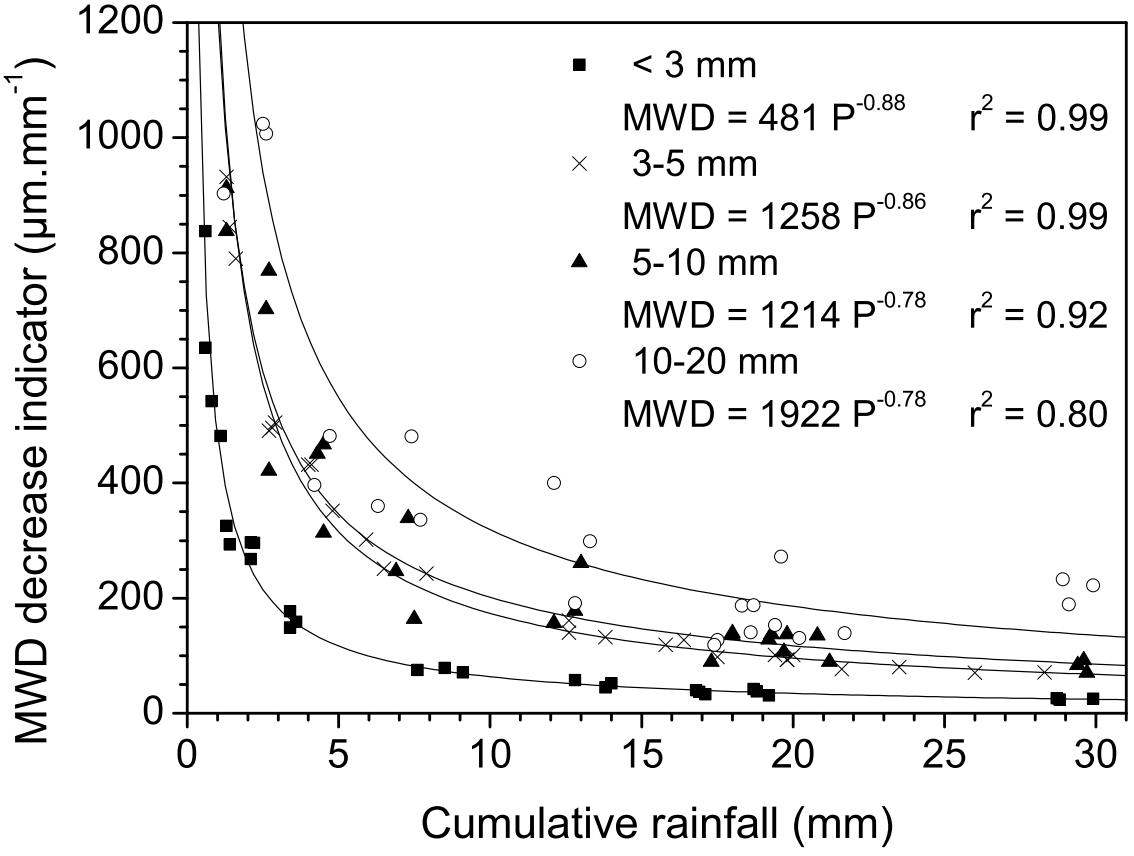
MWD decrease indicator (µm.mm-1)
Cumulative rainfall (mm)
< 3 mm
MWD = 481 P-0.88 r2 = 0.99
3-5 mm
MWD = 1258 P-0.86 r2 = 0.99
5-10 mm
MWD = 1214 P-0.78 r2 = 0.92
10-20 mm
MWD = 1922 P-0.78 r2 = 0.80

(b)

Figure 6

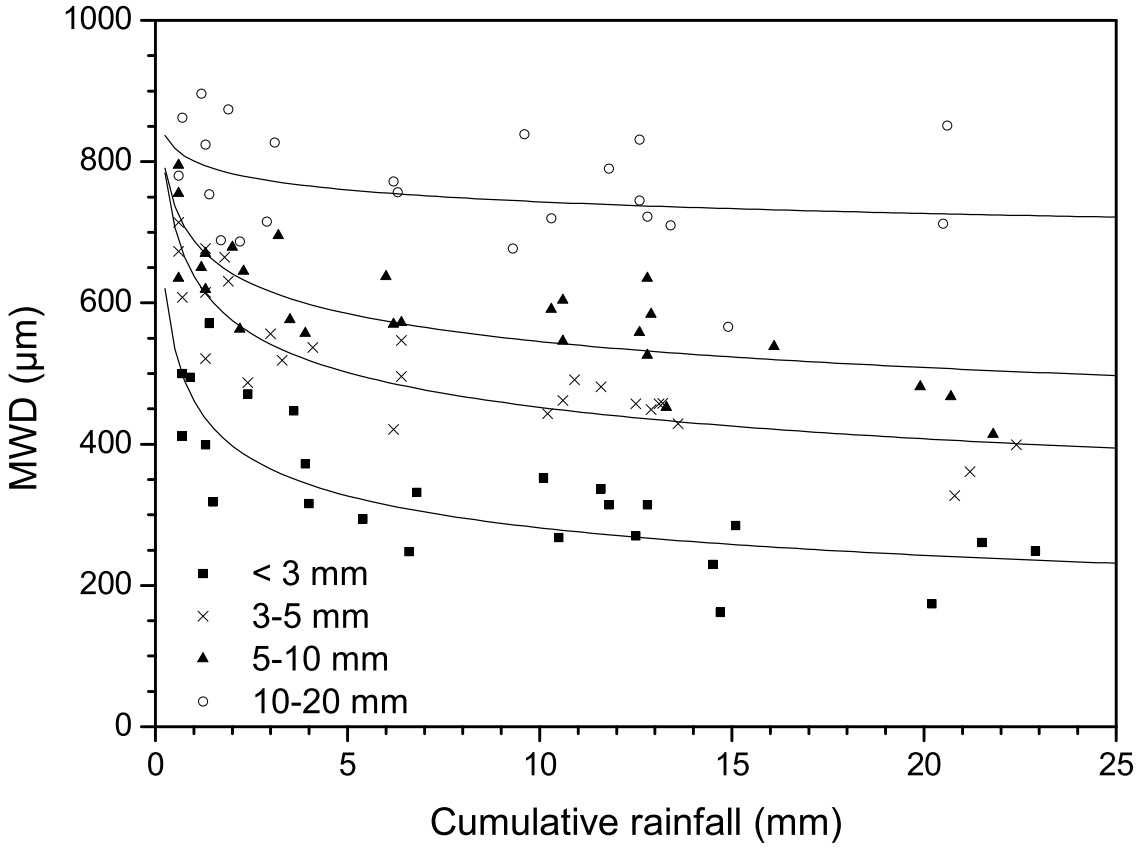
1000
800
600
400
200
0
MWD (µm)
< 3 mm
3-5 mm
5-10 mm
10-20 mm
0
5
10
15
20
25
Cumulative rainfall (mm)

(a)

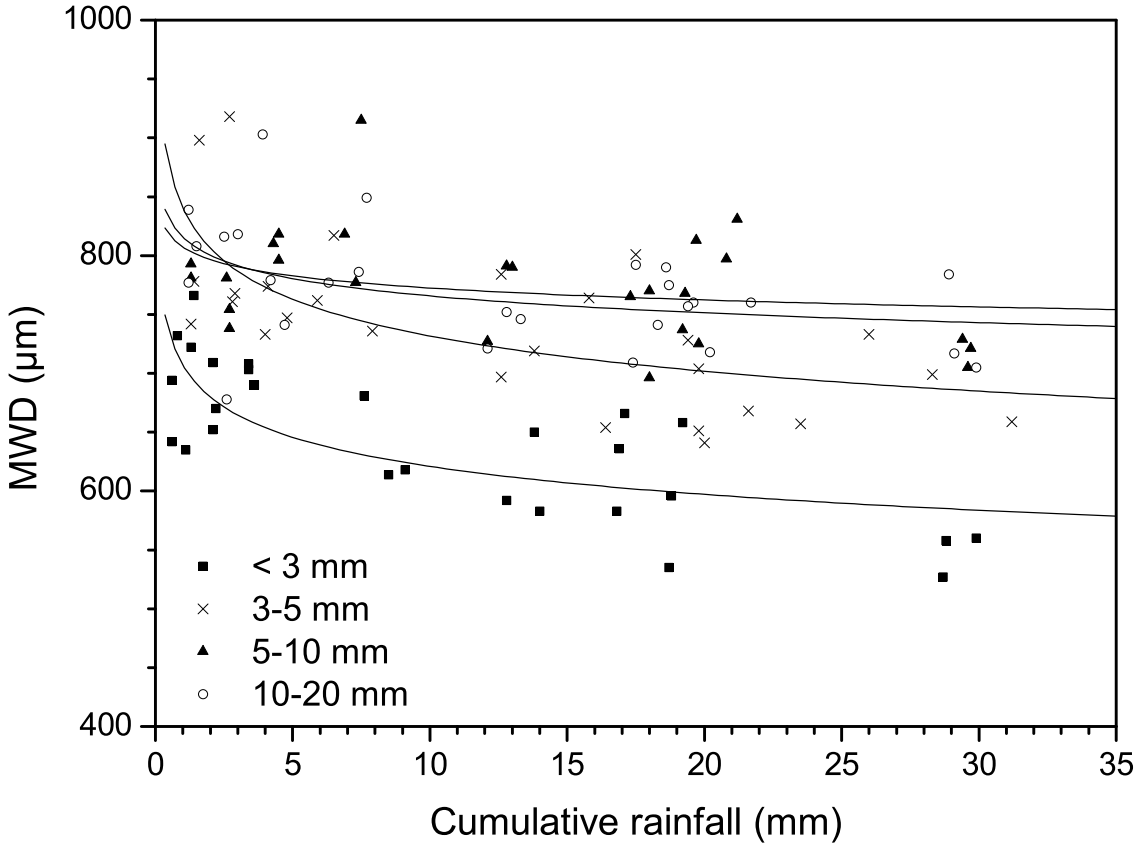
1000
800
600
400
MWD (µm)
< 3 mm
3-5 mm
5-10 mm
10-20 mm
0
5
10
15
20
25
30
35
Cumulative rainfall (mm)

(b)

Figure 7

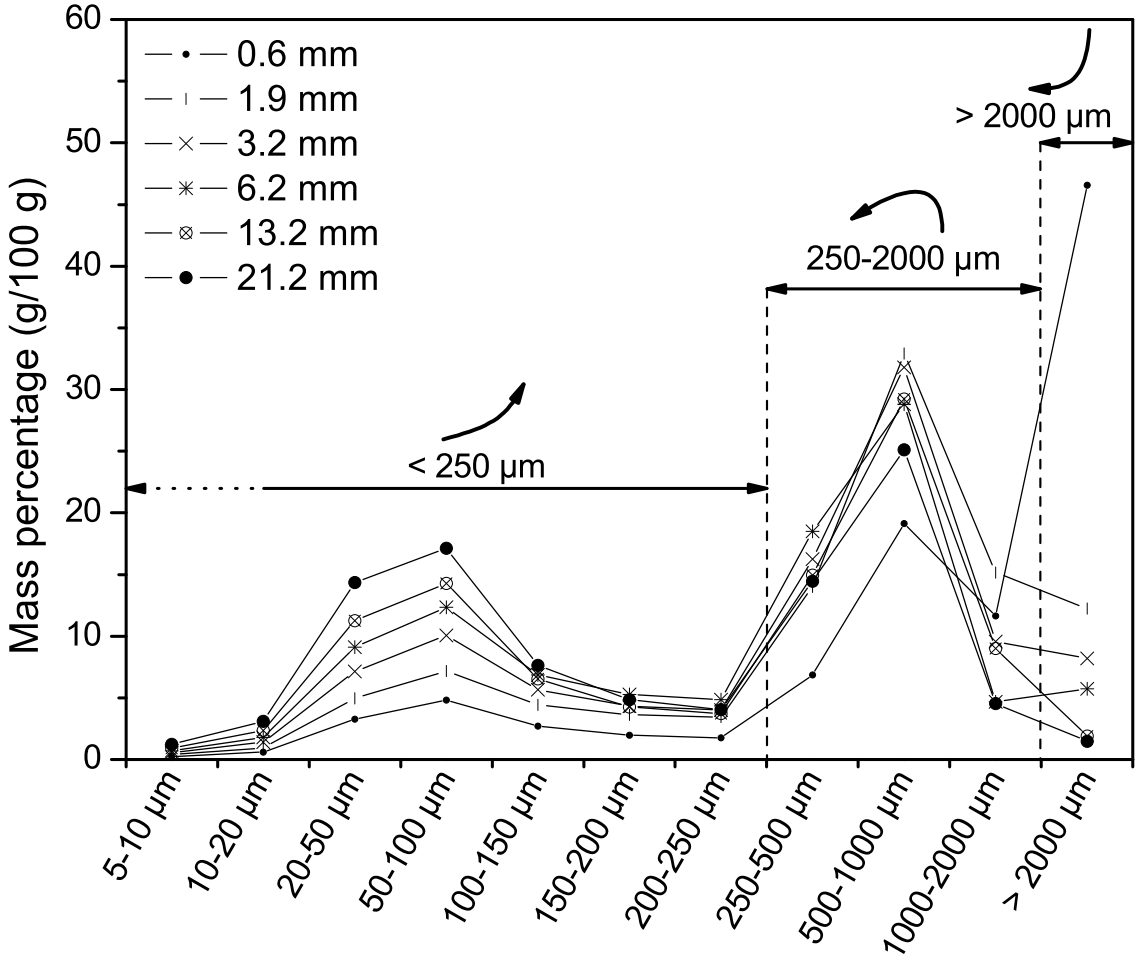
0.6 mm
1.9 mm
3.2 mm
6.2 mm
13.2 mm
21.2 mm
< 250 µm
250-2000 µm
> 2000 µm
Mass percentage (g/100 g)
0
10
20
30
40
50
60
5-10 µm
10-20 µm
20-50 µm
50-100 µm
100-150 µm
150-200 µm
200-250 µm
250-500 µm
500-1000 µm
1000-2000 µm
> 2000 µm

(a)

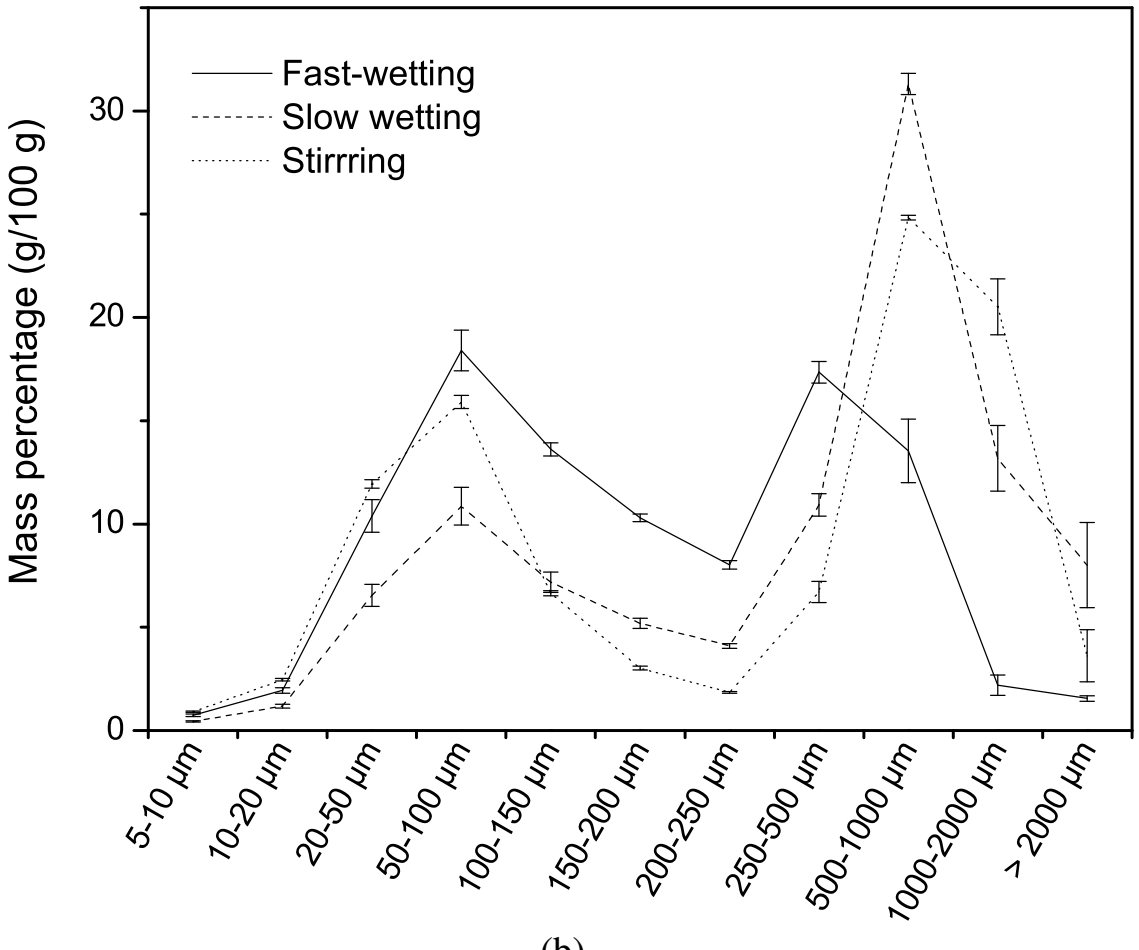
Fast-wetting
Slow wetting
Stirrring
Mass percentage (g/100 g)
0
10
20
30
5-10 µm
10-20 µm
20-50 µm
50-100 µm
100-150 µm
150-200 µm
200-250 µm
250-500 µm
500-1000 µm
1000-2000 µm
> 2000 µm

(b)

Figure 8

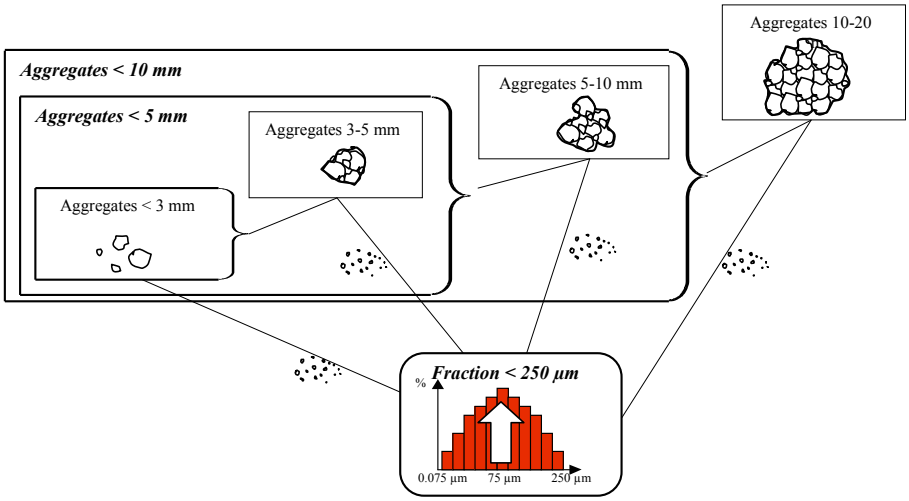
Aggregates 10-20
Aggregates < 10 mm
Aggregates 5-10 mm
Aggregates < 5 mm
Aggregates 3-5 mm
Aggregates < 3 mm
Fraction < 250 µm
%
0.075 µm
75 µm
250 µm

Figure 9

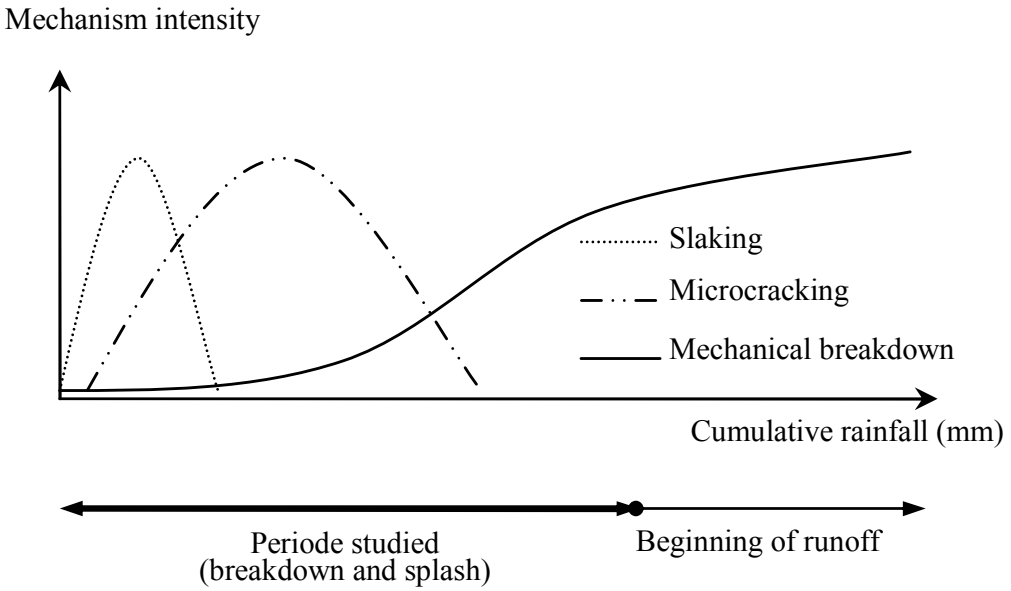
Mechanism intensity
Slaking
Microcracking
Mechanical breakdown
Cumulative rainfall (mm)
Periode studied
(breakdown and splash)
Beginning of runoff

(a)

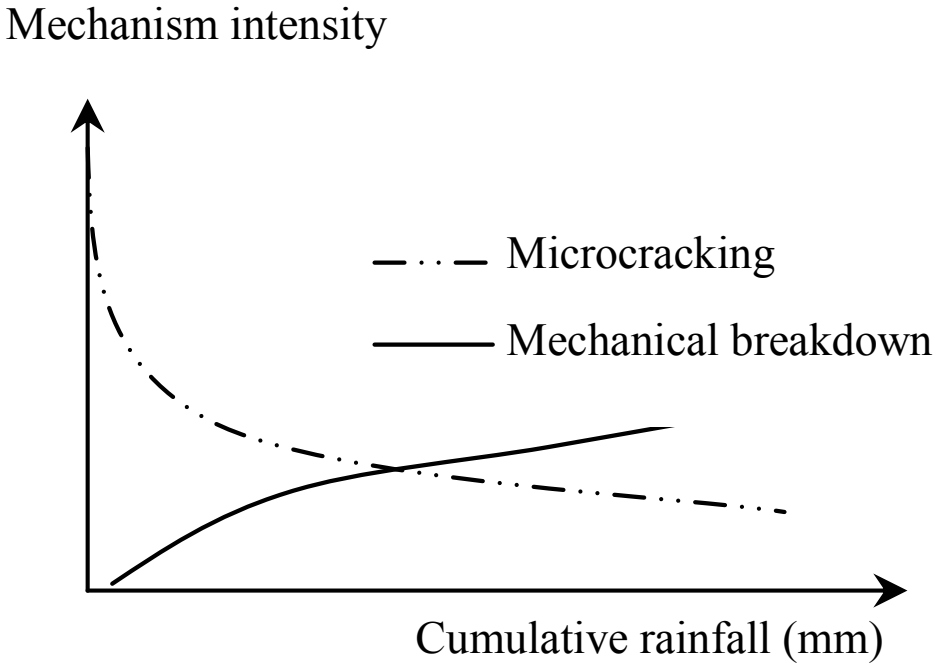
Mechanism intensity
Microcracking
Mechanical breakdown
Cumulative rainfall (mm)

(b)

Figure 10

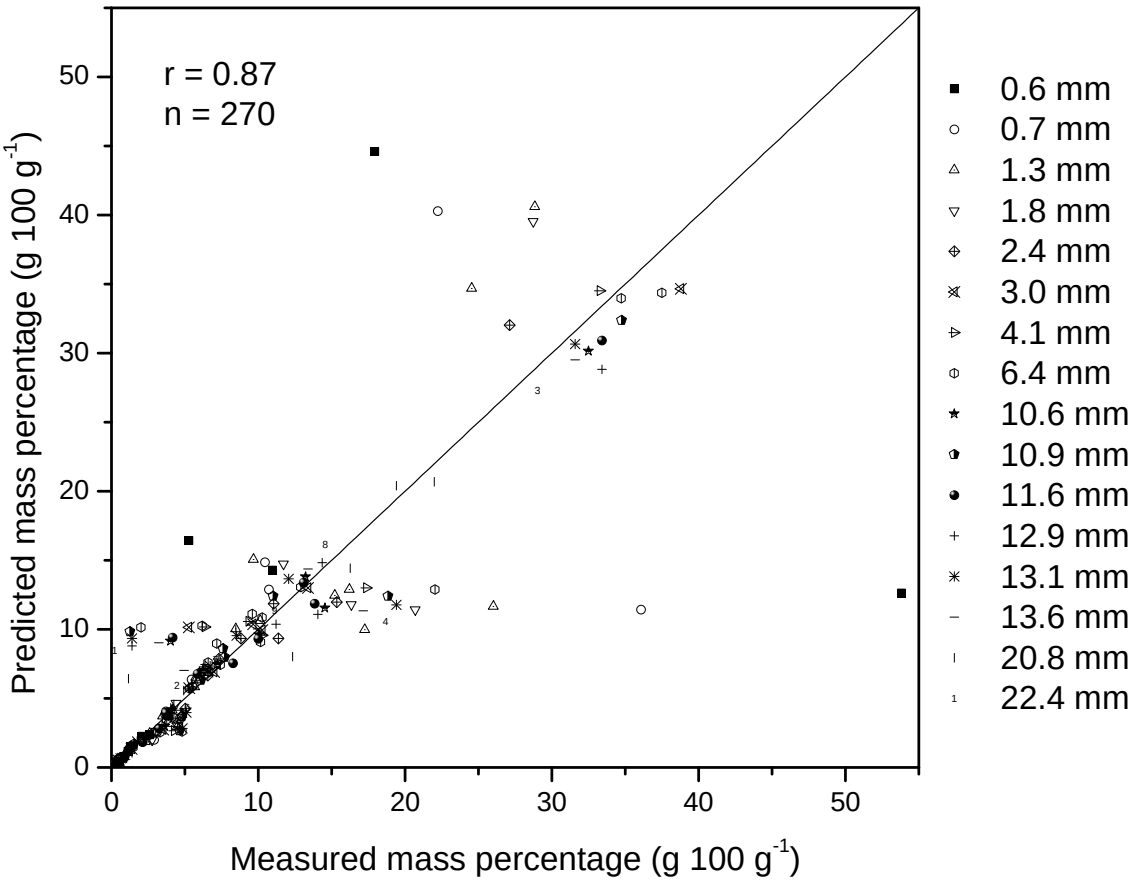
r = 0.87
n = 270
Predicted mass percentage (g 100 g-1)
Measured mass percentage (g 100 g-1)
0
10
20
30
40
50
0.6 mm
0.7 mm
1.3 mm
1.8 mm
2.4 mm
3.0 mm
4.1 mm
6.4 mm
10.6 mm
10.9 mm
11.6 mm
12.9 mm
13.1 mm
13.6 mm
20.8 mm
22.4 mm

Figure 11